Key Engineering Materials Vols. 396-398 (2009) pp 539-542
online at http: www.scientific.net

Online available since 2008/Oct/21

Internal distribution of several inorganic microparticles in mice

Shigeaki Abe[1, *], Chika Koyama[2], Tsukasa Akasaka[1], Motohiro Uo[1], Yoshinori Kuboki[2, 3] and Fumio Watari[1]

[1]Department of Biomedical Materials and Engineering, Graduate School of Dental Medicine, Hokkaido University, North 13, West 7, Kita-ku, Sapporo 060-8586, Japan

[2]School of Dental Medicine, Hokkaido University, North 13, West 7, Kita-ku, Sapporo 060-8586, Japan

[3] *Koken Bioscience Institute, 2-13-10 Ukima, Kita-ku, Tokyo 115-0051, Japan*

[*]sabe@den.hokudai.ac.jp

Keywords: biodistribution, microparticle, visualization, X-ray scanning analytical microscopy

Abstract.

Internal distributions of several inorganic microparticles administered into the tail vein of mice were determined using a Scanning X-ray analytical microscopy and energy-dispersed X-ray spectroscopy. After administration through the tail vein of mice, the particles circulated by blood flow then reach some organs and temporally remained. In this study, we determined that the distribution behaviors in body depend upon the chemical species and the size.

Introduction

Recently, micro- / nano-sized inorganic- materials have received much attention in view of biocompatibility and / or nanotoxicity because of developments in nanotechnology. When the size of particles reaches the micro/nano level, some of them have shown toxicity *in vitro* even they are considered biocompatibile at the macro level [1-5]. In previous study, we determined that even biocompatible materials such as Ti and TiO_2 cause inflammation with the decrease of particle size [5]. To investigate the compatibility, it is important to determine the internal distribution of the materials in body. Some investigators have reported the biodistribution of micro- / nano- particles. Moritake et al. reported *in vivo* delivery of nano-magnetic particles by external magnetic field [6]. Ballou et al. determined and visualized surface modified Quantum dots by their strong emission [7]. However, the distributions of other biocompatible materials particles are still unknown. In addition, the method for distribution analysis without labeling is able to avoid the effect of labeling to distribution. Recently, we determined the biodistribution of Pt and TiO_2 microparticles in mice using X-ray scanning analytical microscopy [8]. This method required no labeled or treatment of target particles. Then, it would be one of the useful methods of the study of biodistribution of micro/nano particle. In the study, Pt microparticles, which have a diameter of 1 μm, quickly circulated in body after injection, then condensed in the spleen. This tendency is in good agreement to typical small molecules. On the other hands, TiO_2 particles (ϕ = 1 μm) were trapped in the lung temporally then remained for a week. In this paper, we described the results of determination that the distribution of several administered inorganic particles in mice using an X-ray scanning analytical microscope and energy-dispersed X-ray spectroscopy.

Materials and Methods

Male mice (Jcl:ICR) were used at ages from 8 to 12 weeks. Several sizes of inorganic particles were obtained. Some of metal microparticles (Fe, Ni, Ti, W etc.) have a diameter less than 10 μm. Pt and TiO_2 (**a**) have a diameter of 1 μm. Fe_2O_3, TiO_2 (**b**) and TiC have a diameter of 0.5 μm. These

particles dispersed into normal saline, respectively. The concentration was adjusted to 10 mg/mL. 0.6 mL of the dispersion was injected into the tail veins of mice. Their organs were excised at several post injection time (from 0 hr. to 2 weeks). The specimens of excised organs were subjected to elemental distribution analysis using X-ray scanning analytical microscope (XGT-2000V, Horiba, Kyoto, Japan). The XSAM observation was carried with the incident X-rays generated from an Rh anode under conditions of 30kV and 1 mA [9-12]. The elemental distribution images in these specimens were also observed by energy-dispersed X-ray spectrometry (EDS) (Genesis, EDAX Japan, Tokyo, Japan). In order to evaluate the concentration of microparticles in the organs, a part of each organ was calcined at 800 °C for 2 hours in air and dissolved in nitrohydro chloric acid (for Pt) or conc. HCl aq. (for TiO_2). The concentrations in the solutions were quantitated with inductively coupled plasma - atomic emission spectroscopy (ICP-AES P-4010, Hitachi, Tokyo, Japan) and the concentrations in each organ were estimated. All operations on animals were in accord with institutional animal use and care regulations of Hokkaido University.

Results and Discussions

Transmission X-ray and the elemental distribution images (Ti) of administered titanium oxide (ϕ = 1μm) of a whole mouse were determined with XSAM (Figure 1). Fluorescence X-ray from Ti in the lung and liver was observed. The fluorescence X-ray in the lung was observed for a couple of days then disappeared, then the fluorescence in the liver was increased with the time. In contrast, fluorescence X-ray from Fe in the lung was observed only in the initial period by Fe_2O_3 particles injection. The fluorescence quickly decreased with post-injection time, and then disappeared after one day. It was suggested that the Fe_2O_3 particles left from lung quickly by blood circulation then arrived at liver. This phenomenon was similar to a typical small molecule. Therefore, the administered particles would be trapped in small tissue such as alveolus, sinusoidal capillary or splenic sinus in organs. In longer time-scale, the total amount of adnministered particles were decreased with post-injection time. Then, the administered particles were considered to be excreted. Our recent work that the concentration of administered Pt microparticles in mice was estimaed with ICP-AES analysis was also suggested the assumption [8].

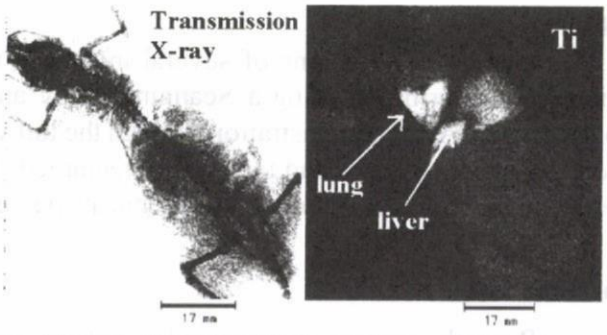

Figure 1. Elemental distribution images (Ti) of mice that was administerd TiO_2 (1) particles at 1 day post-injection.

To determine the details of the distribution in the organs, speicimens of the lung administered TiO_2 particles were prepared then observed by EDS. As shown in Figure 2, the administered TiO_2 particles were localized in the lung. They would distribute along the lung tissue. In other organs, no graphical patterned distribution, such as Figure 2b, were observed. However, the distribution as a un-natural dotted manner was observed in some organs.

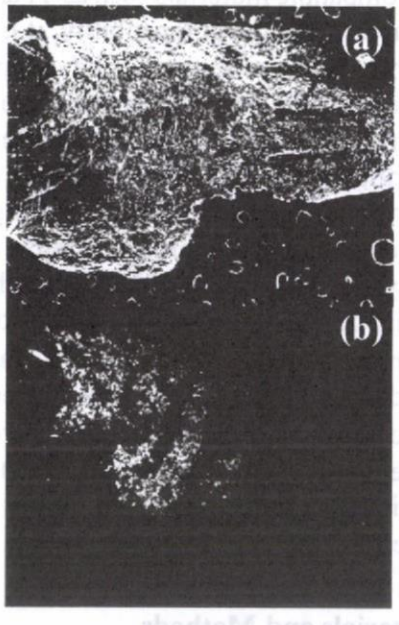

Figure 2. SEM (a) and EDS (b) images (Ti) in the lung of mice that was administerd TiO_2 (1) particles at 1 day post-injection.

To confirm the difference of deponded upon the

chemical spieces, several inroganic microparticles were administered into mice. The speicemens that were excised the mice's organs (lung, liver, kidney and spleen) after microparticles injection were observed with XSAM. The distributions of administered particles in body at 1 day post-injection were determined as shown in Figure 3. The distribution in body varied with the materials. In addition, the distribution changed when the size of particle was different. The result suggests that the biodistribution depend upon not only the materials but also the size of particles. According our previous study, the distribution is in good agree to the relative concentration of injected particles in the organs. The distribution of inorganic microparticles in body were breifly distinguished 2 types. One is condensed in the lung, another is condensed in the spleen. Now, we do not arrive the clear mechanism, however, some of particles show a time-dependence of the biodistribution. For example, TiO_2 and Pt microparticles, which have a diameter of 1 μm, show clearly different time-dependence of the biodistribution [8]. The injected Pt particles reachs in the lung at first, then move to other organs rapidlly. On the other hands, TiO_2 particles are temporaly trapped in the lung and remeined for a week. This result suggests that the administered inroganic microparticles have different distribution in body depending upon the elements, even they have same diameter. Therefore, it is important to investigate the biodistribution of several materials in body.

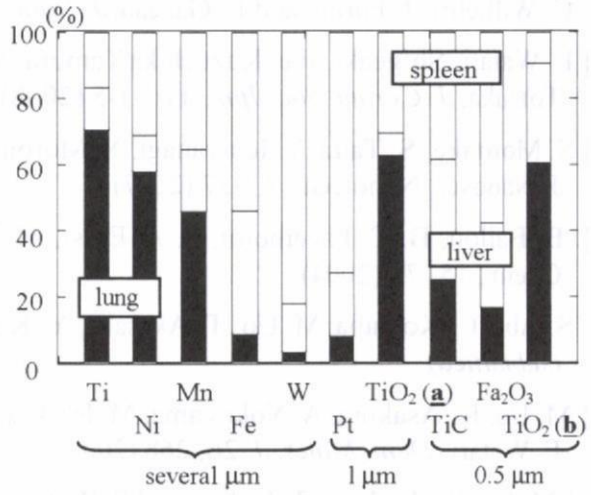

Figure 3. Relative concentration of administered several inogranic microparticles in the lung, liver and spleen of mice at 1 day post-injection.

These results suggested that each administered material had the individual distribution property and some of them showed their time-dependence. In addition, it was suggested that the distribution of particles was depended on the particle size.

Summary

In this study, we succeeded to visualize of biodistribution of inorganic microparticles in mice. The difference from chemical species and the effect of particle size for the distribution were determined. We also succeeded to observe the localized unique distribution in the tissue using an energy-dispersed X-ray spectroscopy.

Acknowledgment

This work was supported by Grant-in-aid for Research on Chemical Substance Assessment from Health and Labor Science Research Grants from the Ministry of Health, Labor and Welfare, Japan (H18-Chemistry-General-006) and Grant-in-Aid for Young Scientists (B) No. 19791419 from the Ministry of Education, Culture, Sports, Science and Technology, Japan.

References

[1] J. Veranth, E. Kaser, M. Veranth, M. Koch, G. Yost, *Particle Fibre Toxicol.*, *4*, 1 (2007).

[2] J. C. Carrero-Sanchez, A. L. Elias, R. Mancilla, G. Arrellin, H. Terrones, J. P. Laclette and M. Terrones, *Nano Lett.*, 6, 1609 (2006).

[3] S. Kim, Y. T. Lim, E. G. Soltesz, A. M. Grand, J. Lee, A. Nakayama, J. A. Parker, T. Mihaljevic, R. G. Laurence, D. M. Dor, L. H. Cohn, M. G. Bawendi and J. V. Frangionor *Nature Biotech.*, *22*, 93 (2004).

[4] C. Wilhelm, J. Fortin, and F. Gazeau, *J. Nanosci. Nanotech.*, 7, 2933 (2007).

[5] F. Watari, Shigeaki Abe, Kazuchika Tamura, Motohiro Uo, Atsuro Yokoyama, and Yasunori Totsuka, *J. Ceram. Soc. Jpn.*, 116, 1-5 (2008)

[6] S. Moritake, S. Taira, Y. Ichiyanagi, N. Morone, S. Song, T. Hatanaka, S. Yuasa and M.Setou, J. Nanosci. Nanotech., 7, 937 (2007)

[7]. B. Ballou, B. C. Lagerholm, L. A. Ernst, M. P. Bruchez and A. S. Waggoner, Bioconjugate Chem., 15, 79 (2004)

[8] S. Abe, C. Koyama, M. Uo, T. Akasaka, Y. Kuboki and F. Watari, *J. Nanosci. Nanotech., (submitted)*

[9] M. Uo, K. Asakura, A. Yokoyama, M. Ishikawa, K. Tamura, Y. Totsuka, T. Akasaka and F. Watari, *Dent. Mater. J.* 26, 268 (2007)

[10] M. Uo, K. Asakura, T. Kohgo and F. Watari, *Chem. Lett.*, 35, 66 (2006)

[11] M. Uo, M. Tanaka and F. Watari, *J. Biomed. Matter. Res. Part B: Appl. Biomater.* 4, 70B, 146 (2004)

[12] M. Uo, F. Watari, A. Yokoyama, H. Matsuno and T. Kawasaki, *Biomaterials*, 22, 1787 (2001)

Journal of Electron Microscopy **57(5)**: 159–164 (2008)
doi: 10.1093/jmicro/dfn016

Physical: Full-length

High-resolution electron microscopy of multi-wall carbon nanotubes in the subcutaneous tissue of rats

Norihito Sakaguchi[1,*], Fumio Watari[2], Atsuro Yokoyama[2] and Yoshinobu Nodasaka[2]

[1]Center for Advanced Research of Energy Conversion Materials and [2]Graduate School of Dental Medicine, Hokkaido University, Kita13, Nishi7, Kita-ku, Sapporo 060-8586, Japan
*To whom correspondence should be addressed. E-mail: sakagu@ufml.caret.hokudai.ac.jp

Abstract The atomic structure of multi-wall carbon nanotubes (MWCNTs) implanted in the subcutaneous tissue of rats was examined by means of high-resolution transmission electron microscopy (HRTEM). Clusters of the MWCNTs implanted in the subcutaneous tissue were well recognized by the TEM observations. It was indicated that some nanotubes were taken in phagocytes after the 1-year implantation. The deterioration of crystalline structure of the nanotubes in phagocytes was shown by the HRTEM observation. It was suggested that the deterioration of the nanotubes was due to the peeling of the outer graphene layers in the phagocytes.

Keywords carbon nanotube, *in vivo*, high-resolution electron microcopy, low-voltage and high-voltage transmission electron microscope

Received 18 August 2008, accepted 20 August 2008

Introduction

The development of nanomaterials for drug delivery systems has attracted considerable attention because of the realization of health promotion and quality of life in the aged society of the 21st century. In particular, many researches for the application of biotechnology of carbon nanomaterials such as carbon nanotubes (CNTs) [1–6], carbon nanofibers (CNFs) [7,8] and fullerenes [9–14] have been extensively performed. Most these researches were due to the *in vitro* examination in the cell culture on scaffolds. Recently, toxicity of CNTs has been reported, and there are a lot of questions about their safety as the biomaterials [15–18]. Therefore, it is especially important to evaluate their toxicity and biocompatibility of the *in vivo* tissue reaction to these nanomaterials. However, there are only a few reports on the biological reaction to the nanoscale materials [19,20]. Yokoyama *et al.* [20] have clarified the tissue response to the CNFs implanted in the subcutaneous tissue of rats by means of transmission electron microscopy (TEM). They concluded that the CNFs in the subcutaneous tissue did not induce an acute severe inflammatory reaction. On the other hand, it was also indicated that the length of the CNFs reduced with time, and some of CNFs were translucent due to the delamination of the graphene layer. However, a deterioration mechanism and an atomic structure of the carbon nanomaterials in the tissue have not been clarified yet. In this paper, we present electron microscopy results on the morphology and crystallography of CNTs implanted in the subcutaneous tissue of rats. High-resolution TEM (HRTEM) was used to investigate the detailed atomic structure of the CNTs in the tissue. The deterioration of the CNTs was also examined by the HRTEM observation.

Materials and methods

Purification, cutting and separation of MWCNTs

Multi-wall CNTs (MWCNT) of about 5 nm in diameter and 0.8 μm in length, synthesized by chemical vapor deposition (NanoLab, Inc., MA, USA.), were used throughout the experiments. The purity of the MWCNTs was 80 wt% with impurities such as amorphous carbon, Fe, Mo, Cr and Al. The diameter was in the range between 20 and 40 nm, and the length was in the range between 500 nm and 5.0 μm. After purification by the method described in a previous report [21], MWCNTs with 98 wt% pure were suspended in a 3:1 mixture of concentrated H_2SO_4/HNO_3, exposed to ultrasonic irradiation and filtered using polycarborbonate membrane filters with respective cylindrical pore diameters of

2.0, 1.2, 0.8 and 0.4 μm. We used the filtered cake samples on 0.8-μm pore size membrane filters as testing samples.

Animal experiments

Incisions were made bilaterally in the thoracic region of six male 6-week-old Wistar strain rats under general anesthesia. Two pockets were made in the subcutaneous tissue. Clusters of MWCNTs were implanted in the subcutaneous tissue of each rat in the thoracic region bilaterally. Animal experiments were performed in accordance with the *Guide for the Care and Use of Laboratory Animals*, Hokkaido University Graduate School of Dental Medicine.

TEM specimen preparation

The rats were sacrificed at 1 week and 1 year after the surgery. Segments of the subcutaneous tissue including the MWCNTs were excised and fixed. TEM specimens were post-fixed with 1% OsO_4 and embedded in epoxy resin after dehydration. Ultrathin sections (80 nm approximately) were cut with a diamond knife and stained with uranyl acetate and lead citrate. Stained sections were placed on a supporting carbon mesh grid.

TEM observation

High-contrast observation of the subcutaneous tissue and the MWCNTs was carried out using a conventional 200 kV TEM (Hitachi H-700) operating at a voltage of 75 kV. A high-resolution high-voltage TEM (HRHVTEM, JEOL JEM-ARM-1300) was used for HRTEM observation of the MWCNTs in the tissue. The spherical and chromatic aberration coefficients of the objective lens of the HRHVTEM were 2.65 and 4.1 mm, respectively. The point-to-point resolution measured at a Scherzer defocus of −53 nm and an acceleration voltage of 1250 kV was 0.118 nm.

Results

Cell organelles of the stained ultrathin section of subcutaneous tissue of rats after MWCNTs' implantation at 1 week and 1 year are shown in Fig. 1. These observations were performed using a low-voltage TEM. Some clusters of MWCNTs were observed as black contrasts in intercellular space both at 1 week and 1 year after the implantation. The structure of large clusters of the MWCNTs unchanged between the 1-week and 1-year implantation, although the degree of aggregation of the clusters slightly decreased after the 1-year implantation. Each organelle was clearly seen in the figure, so severe inflammatory response such as necrosis might be very weak in both cases. The magnified TEM images of the MWCNTs implanted in the subcutaneous tissue at 1 week and at 1 year are shown in Fig. 2. Some nanotubes separated from the cluster of the MWCNTs after the implantation at 1 week. The separating nanotubes are not divided into

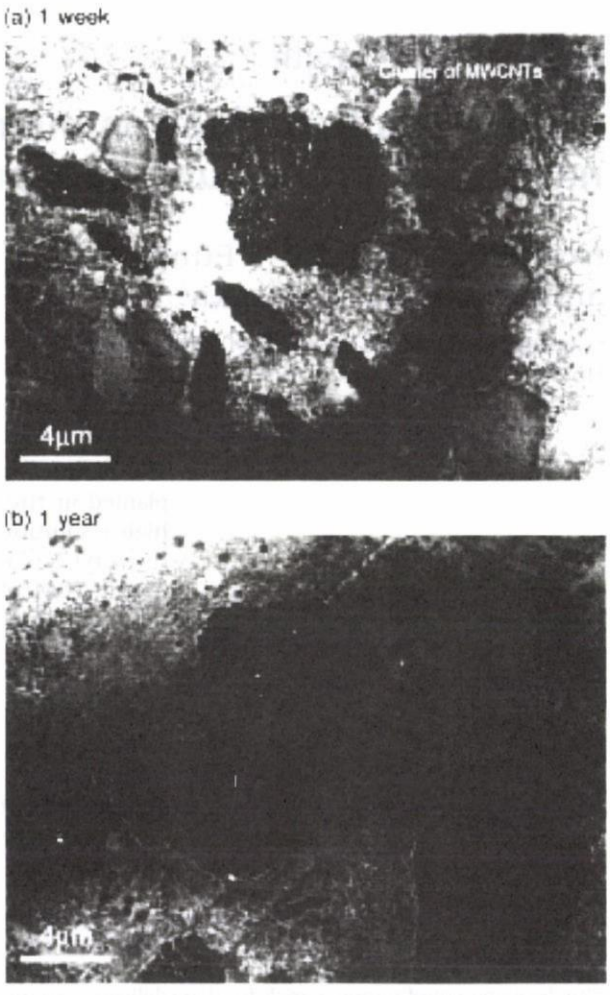

Fig. 1. Cell structures and clusters of MWCNTs implanted in the subcutaneous tissue of rat at (a) 1 week and (b) 1 year.

parts although they are slightly curved. At 1 year after the implantation, some of separating nanotubes were observed in phagocytes with a lot of vacuoles. The mean length of the MWCNTs covered by the lysosomal membranes looks shorter than that observed at a 1-week implantation sample although the characteristic form of the nanotubes was recognized.

To examine the detailed atomic structures of the MWCNTs in the tissue, the HRTEM observations were performed using a high-voltage TEM. Figure 3 shows a bright-field image and HRTEM images of the MWCNTs implanted in the subcutaneous tissue of rats at 1 week. Although the contrasts of the bright-field image on both the cell organelles and MWCNTs were weaker than those of Fig. 2, one can see the morphology and aggregation of individual nanotubes by using the HVTEM. Moreover, although the nanotubes were embedded in the subcutaneous tissue, the stacking of the graphene layers of each nanotube was clearly visible in the HRTEM image. Since the surrounding tissue causes the

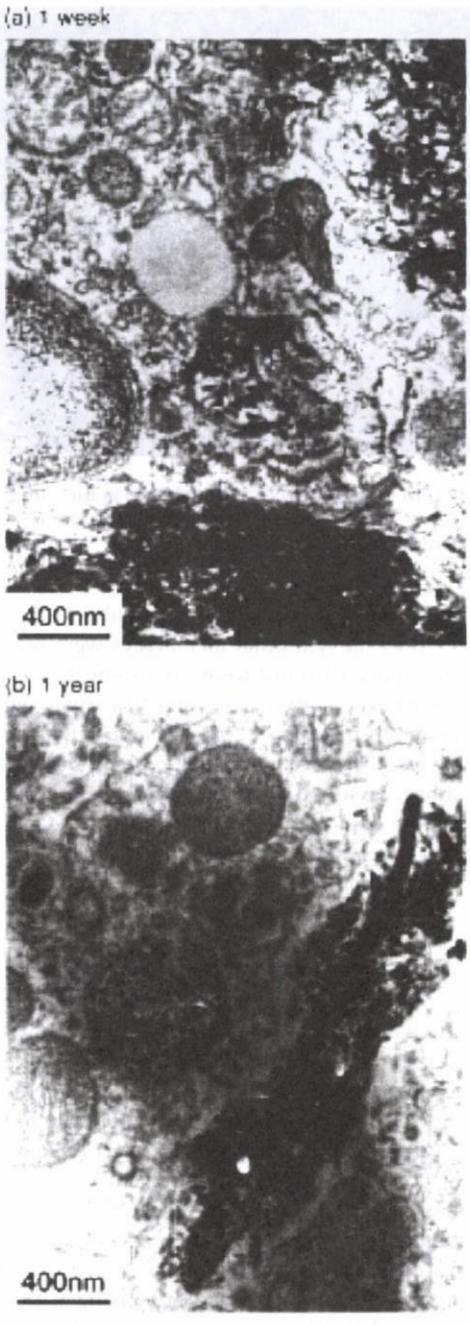

Fig. 2. TEM images of MWCNTs implanted in the subcutaneous tissue at (a) 1 week and (b) 1 year.

deterioration of the quality of the HRTEM image because of the scattering of electrons, this influence can be disregarded by the high-energy electrons due to their high transparency. The observed nanotubes are curved in some places but the layered structure of graphene is entirely kept around there. This implies that the MWCNT could exist in a stable form during the 1-week implantation in the subcutaneous tissue.

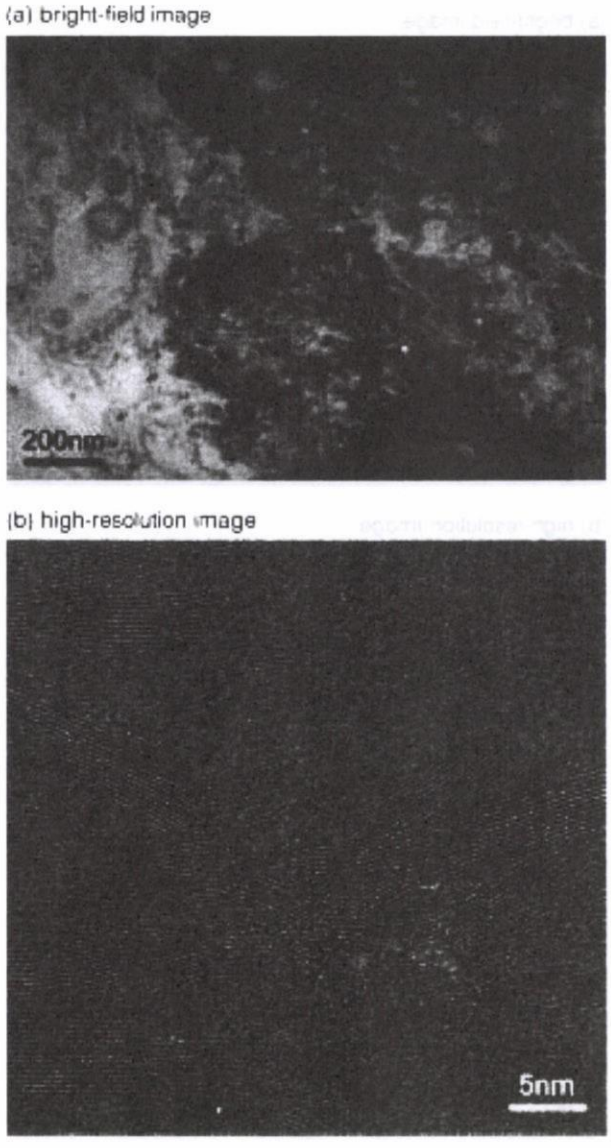

Fig. 3. (a) A bright-field image of MWCNTs implanted in the subcutaneous tissue of rat at 1 week and (b) the corresponding HRTEM images of the MWCNTs.

After 1 year from the implantation, some loose MWCNTs were observed in phagocytes. Figure 4 shows a bright-field image and HRTEM images of the MWCNTs implanted at 1 year. In the bright-field image, although the characteristic form of the MWCNTs was recognized, the contrast of each nanotube was weaker than that shown by the 1-week implantation. In other words, some nanotubes appeared translucent. The atomic structures of the MWCNTs slightly differed from the previously observed structure too. Although stacking of the graphene layers was recognized in the HRTEM image, the atomic structure of the nanotubes was slightly indistinct. In some places, the nanotube was disconnected and slightly waved. A typical HRTEM image

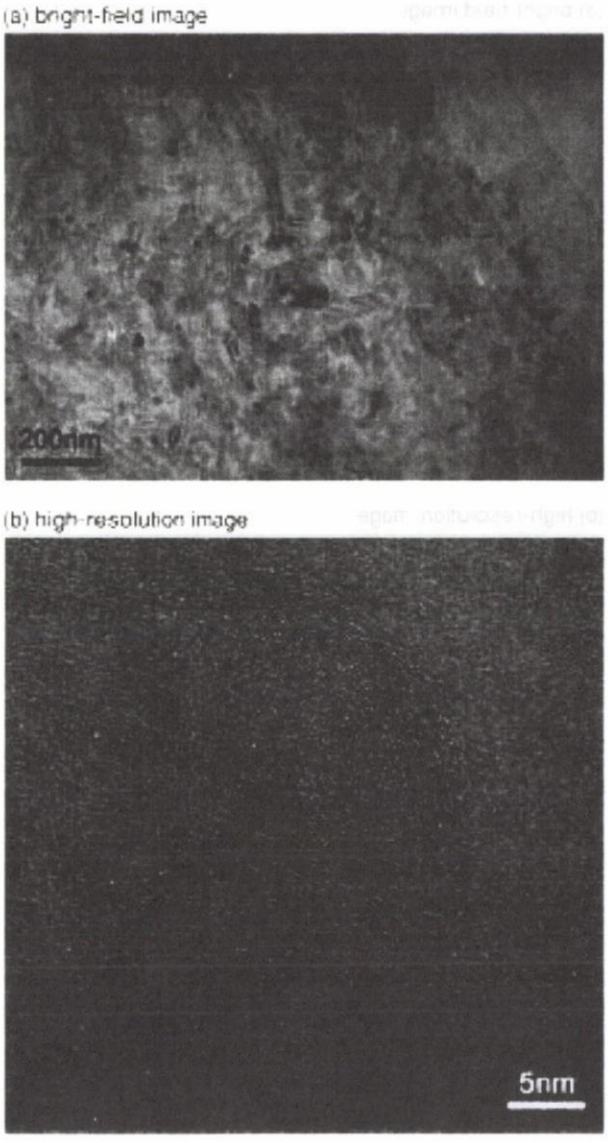

Fig. 4. (a) A bright-field image of MWCNTs implanted in the subcutaneous tissue of rat at 1 year and (b) the corresponding HRTEM images of the MWCNTs.

that indicated the disconnection of the nanotube is shown in Fig. 5. Each break of arc is indicated by white arrows. In particular, deterioration of the nanotube at the edge was remarkable. Such deterioration was seldom seen in the tissue of 1-week implantation.

Discussion

Presently observed clustering of MWCNTs which were implanted in the subcutaneous tissue indicates that the degree of the aggregation of the MWCNTs slightly decreased after the 1-year implantation. At the same time, some of separated nanotubes from the clustered MWCNTs were observed

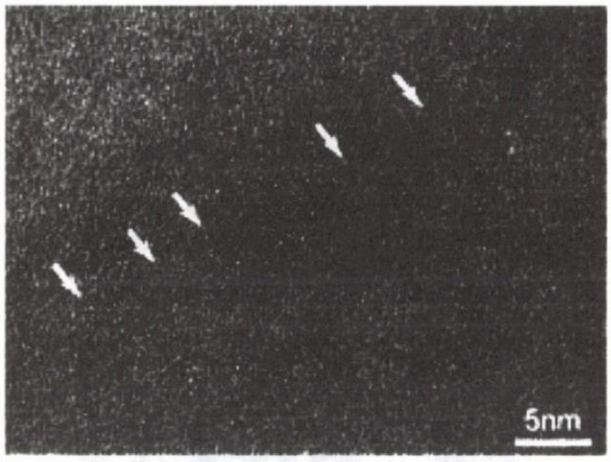

Fig. 5. HRTEM image of a MWCNT implanted in the subcutaneous tissue of rat at 1 year. The arrows indicate the deterioration sites of the graphene layers of the MWCNT.

in lysosomes after the 1-year implantation. The MWCNTs covered by the lysosomal membranes were reduced in length and appeared translucent. The same tendency has been reported by Yokoyama *et al.* on CNFs implanted in the subcutaneous tissue of rats [20] concluding that the structural changes which occurred in lysosomes and cytoplasm were attributable to the delamination of the graphene layers due to the intercalation of hydrophilic substances such as enzymes and proteins in the phagocytes. Delamination by the intercalation reactions was also reported elsewhere [22,23]. The deterioration behavior of the graphene layers in the MWCNT was first reported by Ajayan *et al.* [24]; peeling of the graphene layers that started from the edge of the MWCNT in an oxidation atmosphere was followed by thinning of the nanotube. In our HRTEM observation, the deterioration of the MWCNT was remarkable at the edge of the nanotube too as shown in Fig. 5. In both, the peeling reaction of the graphene layers commonly initiated at the edge of the nanotube. In some cases, however, structural damages of the MWCNT were observed not only at the edge but also in the outer graphene layer of the nanotube. Similar deterioration in the outer graphene layer has been observed in supercritical water [25,26]. Local hydration or hydro-oxidation, i.e. the newly formed C–H or C–OH bonding with sp^3 hybridization caught by Raman spectroscopy [26], possibly initiates the introduction of the surface damage of the MWCNT. Usually, each carbon atom on a graphene layer bonds with sp^2 hybridization in-plane and π bonding occurs between the individual graphene layers. However, once the sp^3 bonding is formed in the outer graphene layer, it causes a partial peeling of the graphene layer because an electron that contributes to the π bonding is lost. Moreover, the strain field due to the formation of three-dimensional sp^3 bonding might enhance the rehybridization from sp^2 to sp^3 between the neighboring graphene layers and peeling reaction of the outer graphene layer.

The sp^2 hybridization of carbon atoms in the graphene layer is one of the strong and stable bondings and it is not easy to break the network of in-plane σ bonding. However, it is expected that the MWCNTs used in the present study would have open edges and a lot of defect sites in the outer graphene layers because the MWCNTs were exposed in the several acid/alkali solutions such as HCL, NaOH and H_2SO_4–HNO_3 during the purification process. In fact, the MWCNTs after the purification showed the hydrophilic behavior. This provides that the sp^3 hybridization due to the bonding between C–H and C–OH occurred at the outer graphene layers of the MWCNTs used in the present study. Therefore, it is considered that the peeling reaction based on the interaction between the hydrophilic substances and the carbon atoms in the outer graphene layer of MWCNTs occurs with a time passage, even though the nanotubes are put into a comparatively weak oxidation environment like *in vivo*. Observed shortening in the length of the nanotubes could occur subsequently.

Concluding remarks

We performed TEM observations on the morphology and crystallography of MWCNTs implanted in the subcutaneous tissue of rats. HRTEM was used to investigate the detailed atomic structure of the MWCNTs in the tissue. Clusters of the MWCNTs implanted in the subcutaneous tissue were well recognized by the TEM observations. It was indicated that the degree of the aggregation of the MWCNT clusters slightly decreased and some nanotubes were taken in phagocytes. The deterioration of crystalline structure of the nanotubes in phagocytes was emphasized by the HRTEM observation. It was suggested that the deterioration of the nanotubes was due to the peeling of the outer graphene layers in the phagocytes.

Acknowledgements

The authors gratefully thank Professor M. Uo and Dr T. Akasaka for their insights. The authors also acknowledge Mr K. Sugawara for his technical support in the HVTEM observations. This work is supported by Health and Labor Sciences Research Grants in Research on Advanced Medical Technology in Nanomedicine Area from the Ministry of Health, Labor and Welfare of Japan.

References

1 Pantarotto D, Partidos C D, Hoebeke J, Brown F, Kramer E, Briand J P, Muller S, Prato M, and Bianco A (2003) Immunization with peptide-functionalized carbon nanotubes enhances virus-specific neutralizing antibody responses. *Chem. Biol.* **10**: 961–966.

2 Muller J, Huaux F, Moreau N, Misson P, Heilier J F, Delos M, Arras M, Fonseca A, Nagy J B, and Lison D (2005) Respiratory toxicity of multi-wall carbon nanotubes. *Toxicol. Appl. Pharmacol.* **207**: 221–231.

3 Wick P, Manser P, Limbach L K, Dettlaff-Weglikowska U, Krumeich F, Roth S, Stark W J, and Bruinink A (2007) The degree and kind of agglomeration affect carbon nanotube cytotoxicity. *Toxicol. Lett.* **168**: 121–131.

4 Balani K, Anderson R, Laha T, Andara M, Tercero J, Crumpler E, and Agarwal A (2007) *Biomaterials* **28**: 618–624.

5 Raja P M V, Connolley J, Ganesan G P, Ci L, Ajayan P M, Nalamasu O, and Thompson D M (2007) Impact of carbon nanotube exposure, dosage and aggregation on smooth muscle cells. *Toxicol. Lett.* **169**: 51–63.

6 Balani K, Chen Y, Harimkar S P, Dahotre N P, and Agarwal A (2007) Tribological behavior of plasma-sprayed carbon nanotube-reinforced hydroxyapatite coating in physiological solution. *Acta Biomaterialia* **3**: 944–951.

7 Price R L, Waid M C, Haberstroh K M, and Webster T J (2003) Selective bone cell adhesion on formulations containing carbon nanofibers. *Biomaterials* **24**: 1877–1887.

8 McKenzie J L, Waid M C, Shi R, and Webster T J (2004) Decreased functions of astrocytes on carbon nanofiber materials. *Biomaterials* **25**: 1309–1317.

9 Jensen A W, Wilson S R, and Schuster D I (1996) Biological applications of fullerenes. *Bioorg. Med. Chem.* **4**: 767–779.

10 Lin JC and Wu C H (1999) Surface characterization and platelet adhesion studies on polyurethane surface immobilized with C_{60}. *Biomaterials* **20**: 1613–1620.

11 Gonzalez K A, Wilson L J, Wu W, and Nancollas G H (2002) Synthesis and *in vitro* characterization of a tissue-selective fullerene: vectoring $C_{60}(OH)_{16}$ AMBP to mineralized bone. *Bioorg. Med. Chem.* **10**: 1991–1997.

12 Prylutska S V, Matyshevska O P, Golub A A, Prylutskyy Y I, Potebnya G P, Ritter U, and Scharff P (2007) Study of C_{60} fullerenes and C_{60}-containing composites cytotoxicity *in vitro*. *Mater. Sci. Eng. C* **27**: 1121–1124.

13 Roberts J E, Wielgus A R, Boyes W K, Andley U, and Chignell C F (2008) Phototoxicity and cytotoxicity of fullerol in human lens epithelial cells. *Toxicol. Appl. Pharmacol.* **228**: 49–58.

14 Spesia M B, Milanesio M E, and Durantini E N (2008) Synthesis, properties and photodynamic inactivation of *Escherichia coli* by novel cationic fullerene C_{60} derivatives. *Eur. J. Med. Chem.* **43**: 853–861.

15 Bianco A, Kostarelos K, and Prato M (2005) Applications of carbon nanotubes in drug delivery. *Curr. Opin. Chem. Biol.* **9**: 674–679.

16 Smart S K, Cassady A I, Lu G Q, and Martin D J (2006) The biocompatibility of carbon nanotubes. *Carbon* **44**: 1034–1047.

17 Pulskamp K, Diabate S, and Krug H F (2007) Carbon nanotubes show no sign of acute toxicity but induce intracellular reactive oxygen species in dependence on contaminants. *Toxicol. Lett.* **168**: 58–74.

18 Pulskamp K, Worle-Knirsch J M, Hennrich F, Kern K, and Krug H F (2007) Human lung epithelial cells show biphasic oxidative burst after single-walled carbon nanotube contact. *Carbon* **45**: 2241–2249.

19 Fugetsu B, Satoh S, Iles A, Tanaka K, Nishia N, and Watari F (2004) Encapsulation of multi-walled carbon nanotubes (MWCNTs) in Ba^{2+}-alginate to form coated micro-beads and their application to the pre-concentration/elimination of dibenzo-*p*-dioxin, dibenzofuran, and biphenyl from contaminated water. *Analyst* **129**: 565–566.

20 Yokoyama A, Sato Y, Nodasaka Y, Yamamoto S, Kawasaki T, Shindoh M, Kohgo T, Akasaka T, Uo M, Watari F, and Tohji K (2005) Biological behavior of hat-stacked carbon nanofibers in the subcutaneous tissue in rats. *Nano Lett.* **5**: 157–161.

21 Sato Y, Yokoyama A, Shibata K, Akimoto Y, Ogino S, Nodasaka Y, Kohgo T, Tamura K, Akasaka T, Uo M, Motomiya K, Jeyadevan B, Ishiguro M, Hatakeyama R, Watari F, and Tohji K (2005) Influence of length on cytotoxicity of multi-walled carbon nanotubes against human acute monocytic leukemia cell line THP-1 *in vitro* and subcutaneous tissue of rats *in vivo*. *Mol. BioSyst.* **1**: 176–182.

22 Liu Z, Ooi K, Kanoh H, Tang W, and Tomida T (2000) Swelling and delamination behaviors of birnessite-type manganese oxide by intercalation of tetraalkylammonium ions. *Langmuir* **16**: 4154–4164.

23 Toomey R, Freidank D, and Ruhe J (2004) Swelling behavior of thin, surface-attached polymer networks. *Macromolecules* **37**: 882–887.

24 Ajayan P M, Ebbesen T W, Ichihashi T, Iijima S, Tanigaki K, and Hiura H (1993) Opening carbon nanotubes with oxygen and implications for filling. *Nature* **362**: 522–525.

25 Chang J-Y, Ghule A, Chang J-J, Tzing S-H, and Ling Y-C (2002) Opening and thinning of multiwall carbon nanotubes in supercritical water. *Chem. Phys. Lett.* **363**: 583–590.

26 Park K C, Hayashi T, Tomiyasu H, Endo M, and Dresselhaus M S (2005) Progressive and invasive fictionalization of carbon nanotube sidewalls by diluted nitric acid under supercritical conditions. *J. Mater. Chem.* **15**: 407–411.

Available online at www.sciencedirect.com
ScienceDirect
Acta Biomaterialia 5 (2009) 607–612
Acta BIOMATERIALIA
www.elsevier.com/locate/actabiomat

Brief communication

Capture of bacteria by flexible carbon nanotubes

Tsukasa Akasaka *, Fumio Watari

Department of Biomedical, Dental Materials and Engineering, Graduate School of Dental Medicine, Hokkaido University, Kita 13 Nishi 7, Kita-ku, Sapporo 060-8586, Japan

Received 17 April 2008; received in revised form 18 July 2008; accepted 19 August 2008
Available online 9 September 2008

Abstract

Capture of bacteria with flexible carbon nanotubes (CNTs) was done in vitro. Bundles of single-walled carbon nanotubes (SWCNTs) or multi-walled carbon nanotubes (MWCNTs) was mixed with *Streptococcus mutans*. Precipitation assays and colony-forming unit formation assays showed free *S. mutans* in the solution was significantly decreased by the addition of the CNTs. Observation of the precipitate by scanning electron microscopy showed bacterial adhesion to CNTs. It has been shown that CNTs of different diameters have significantly different effects on the precipitation efficiency, and the manners in which they capture the cells are different. We found that MWCNTs (diameter of approximately 30 nm) had the highest precipitation efficiency, which was attributable to both their adequate dispersibility and aggregation activity. From observations by scanning electron microscopy, bundles of SWCNTs and thin MWCNTs (diameter of approximately 30 nm), which were moderately flexible, were easily wound around the curved surface of *S. mutans*. Bare CNTs having high adhesive ability could be useful as biomaterials, e.g., as tools for the elimination of oral pathogens at the nano-level.

Keywords: Carbon nanotubes; Bacteria; *Streptococcus mutans*; Adhesion

1. Introduction

Many carbon materials exhibit excellent molecular adsorption properties, and activated carbon (AC) [1], which is widely used as an adsorbent, has a high capacity for adsorption owing to its porous structure and large surface area. The occurrence of dental caries is mainly associated with oral pathogens, and *Streptococcus mutans* is a primary cariogenic organism. Therefore, many attempts have been made to eliminate *S. mutans* from the oral cavity. One effective way is to use AC as an adsorbent, hence it is used in a wide range of oral care products, such as toothpastes and mouthwashes [2,3].

Carbon nanotubes (CNTs) have attracted considerable attention because of their unique physical properties and potential for a variety of biological applications [4]. In recent investigations, CNTs have been utilized as adsorbents to eliminate dyes [5]. In addition, CNTs can adsorb bacteria [6–8]; single-walled carbon nanotubes (SWCNTs) exhibit strong antimicrobial activity toward *Escherichia coli* [9,10]. However, bacterial adhesion, particularly oral bacterial adhesion, to CNTs has not yet been sufficiently investigated. If bare CNTs are found to have strong adhesive activity and winding CNTs bind oral pathogens, they may be useful as tools at the nano-level for capturing oral pathogens. In this study, we investigated oral bacterial adhesion to CNTs of different diameters and flexibility, and compared them with the widely used adsorbent AC particles. In general, SWCNTs with diameter of approximately 1 nm are known to be highly flexible, while multi-walled carbon nanotubes (MWCNTs) with diameters >100 nm are hard. Here we report that CNTs with different diameters have significantly different effects on the efficiency of *S. mutans* precipitation, that the manners in which they capture bacteria are different and that bundles of SWCNTs and MWCNTs with average diameters of 30 nm can wind around the curved surfaces of bacteria.

* Corresponding author. Tel./fax: +81 11 706 4251.
E-mail address: akasaka@den.hokudai.ac.jp (T. Akasaka).

1742-7061/$ - see front matter © 2008 Acta Materialia Inc. Published by Elsevier Ltd. All rights reserved.
doi:10.1016/j.actbio.2008.08.014

2. Experimental

The SWCNTs employed were synthesized by an arc discharge method. The MWCNTs used were of two types: 30-MWCNTs (average diameter of 30 nm; produced by NanoLab Inc., Brighton, MA) and 200-MWCNTs (average diameter of 200 nm; produced by MTR Co. Ltd., OH). As a control carbon sample, a commercial activated carbon powder (AC) with an average particle size of 20 μm (Kanto Chemical Co. Inc., Tokyo, Japan) was used in this study. *S. mutans* JC2 was grown aerobically in brain heart infusion (BHI) broth at 37 °C for several days. The bacteria were harvested by centrifugation at 2500*g* (Kubota Centrifuge 2700), washed in phosphate-buffered saline (PBS: 20 mM K_2HPO_4/KH_2PO_4, 150 mM NaCl, pH 7.4) and suspended in the same buffer to an optical density (OD) of 1.0 at 700 nm.

For a bacterial precipitation assay, 6 ml of a suspension of CNTs treated by ultrasonication in PBS was added to 3 ml of the bacterial suspension in a glass bottle. As a control, PBS solution was used in substitution for CNTs solutions (initial OD of final volume was 0.34; 1.4×10^8 colony-forming units (CFU) ml^{-1}). The solution was shaken at 200 rpm for 20 min by a universal shaker (Iwaki SHK-U3) and then centrifuged at 100*g* for 3 min. A 2 ml sample of the upper suspension was transferred to a quartz cell, and the OD at 700 nm was measured with an ultraviolet–visible spectrometer.

To identify the suspended carbon of the supernatant after centrifugation, aliquots of the supernatant at a carbon sample concentration of 0.66 mg ml^{-1} were dried on a slide glass. The dry substances were sputtered using a carbon coater (Meiwa Shoji CC-40F) and then examined by scanning electron microscopy (SEM; Hitachi S4000). For a CFU formation assay of the supernatant after centrifugation, a 1 ml sample of each supernatant carbon sample at concentration of 0.66 mg ml^{-1} was used. Upon serial dilution, the diluted samples (10 μl each in triplicate) were spread evenly onto solid BHI medium plates for aerobic incubation at 37 °C for 3 days, and the colonies were then counted.

For SEM observation of the precipitate after centrifugation, the precipitate was collected on a polycarbonate filter (Advantec, 0.8 μm in pore size) and immersed in a fixative (2% glutaraldehyde in PBS) for 2 h. The samples were dehydrated in graded ethanol and dried with CO_2 in a critical point dryer (Hitachi HCP-1). The cells were sputtered using a carbon coater and then examined by SEM.

3. Results and discussion

The adhesive activities of the CNTs were assessed by a bacterial precipitation assay using *S. mutans*. The results of the precipitation assay are presented in Fig. 1a and b. When the bacterial suspensions were mixed with the CNTs, there was loss in supernatant turbidity with an increase in the amount of CNTs. The results clearly show that CNTs have adhesive ability. These results regarding *S. mutans* adhesion to CNTs are in agreement with the previously reported results regarding bacterial adhesion to CNTs in the case of *E. coli* [7–10]. Among the carbon samples, the precipitation efficiency of 30-MWCNTs was the highest, with a maximum at 0.17 mg ml^{-1} concentration. SWCNTs were less effective because they were not easily dispersed

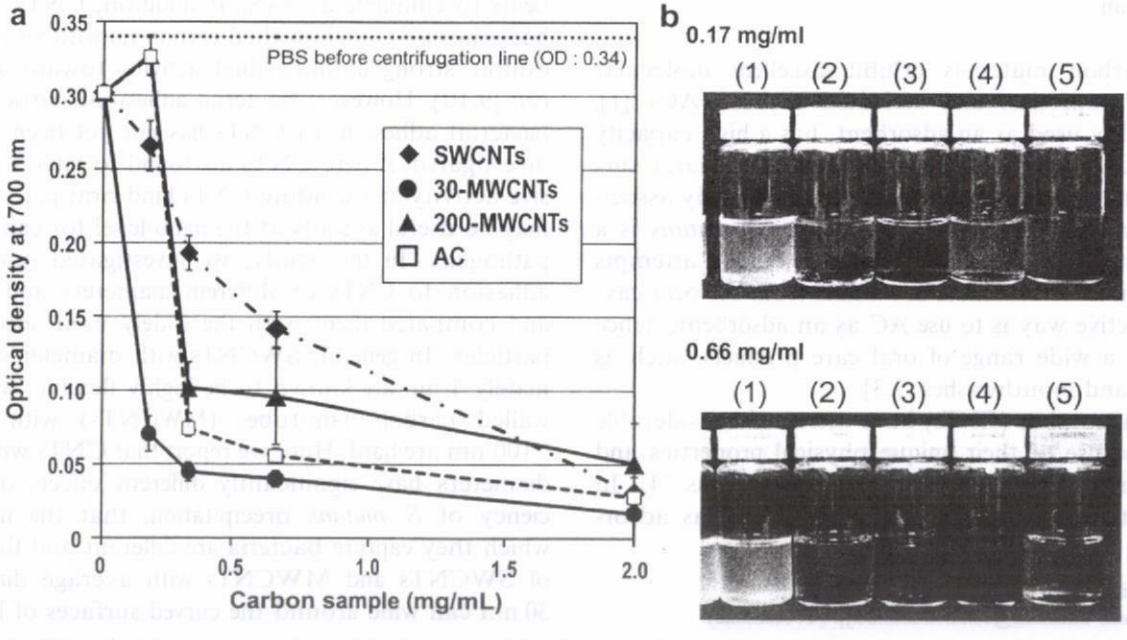

Fig. 1. (a) OD (at 700 nm) of the supernatant in precipitation assay with carbon samples. Results are presented as means ± SE of three experiments. The upper dotted line is the OD value (0.34) of PBS before centrifugation (control). (b) Photographs of *S. mutans* mixed with carbon samples: PBS (b-1); SWCNTs (b-2); 30-MWCNTs (b-3); 200-MWCNTs (b-4); AC (b-5) after centrifugation.

before mixing with the bacteria; and 200-MWCNTs seemed to be less effective because some of them did not precipitate but remained suspended in the solution.

Fig. 2 shows that the number of free *S. mutans* and/or *S. mutans* adhering to suspended carbon samples depends on the type of carbon sample employed. A considerable number of free bacteria were observed with PBS and SWCNTs. However, few free bacteria were observed with 30-MWCNTs, 200-MWCNTs and AC. Moreover, with 200-MWCNTs and AC, a comparatively large amount of suspended carbon was observed. In the AC, small particles (particle size 1–10 μm) were observed in the AC particles. These carbon suspensions occur when bacteria or bacterial products act as surfactants. It was found that 200-MWCNTs were strongly adhesive to bacteria but showed poor precipitation in the bacterial suspension.

To remove the influence of the suspended carbon samples in the supernatant on the assessment of bacterial adhesion, the residual amount of bacteria was evaluated by CFU formation assay. The percentage of CFUs referenced to the control is shown in Fig. 3. The number of free bacteria decreased for all carbon samples, reaching reductions of 65–96% from the initial numbers of bacteria in the suspension. In particular, 30-MWCNTs and 200-MWCNTs bring about the highest decrements, of 92% and 96%, respectively. This result shows that 30-MWCNTs and 200-MWCNTs are highly adhesive to bacteria. However, 200-MWCNTs did not readily precipitate from suspension, a large amount of them remaining suspended in the supernatant (Fig. 2d), with the OD value of the supernatant being comparatively high (Fig. 1).

Kim et al. [7] reported that CNT clusters show high affinity toward and bind *E. coli* cells. No significant

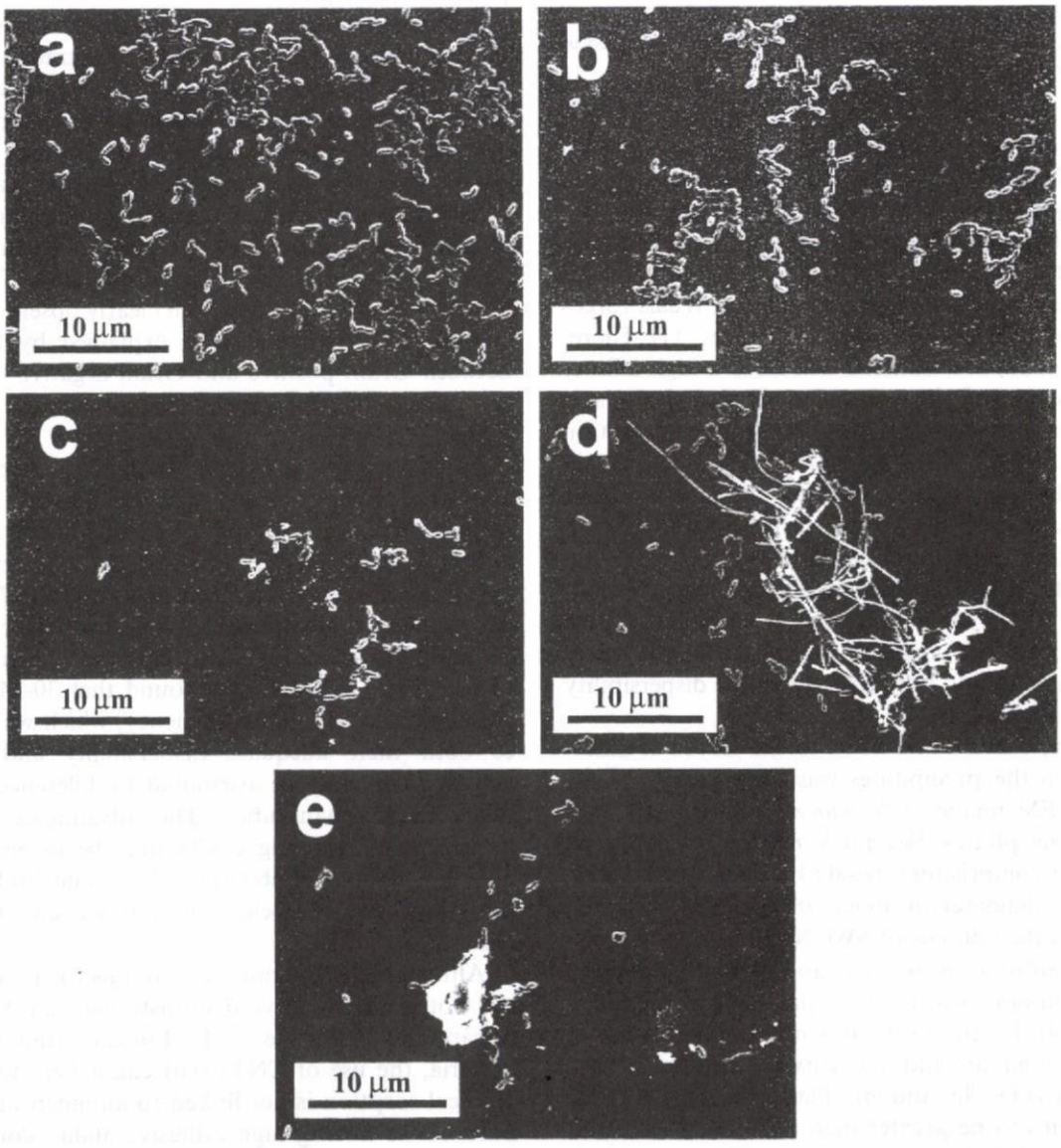

Fig. 2. SEM images of dried supernatant on a slide glass after mixing with carbon samples at a concentration of 0.66 mg ml^{-1}: PBS (a); SWCNTs (b); 30-MWCNTs (c); 200-MWCNTs (d); AC (e).

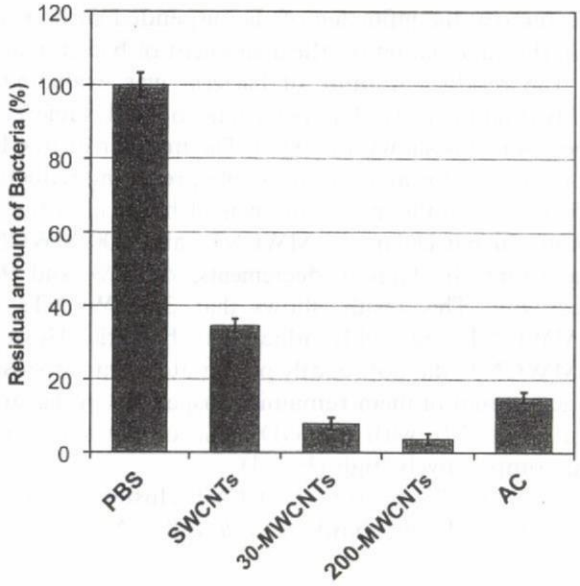

Fig. 3. Residual amount of *S. mutans* in the supernatant after mixing with carbon samples at 0.66 mg ml^{-1} concentration. Results are presented as means ± SE of three experiments.

difference in the affinity of bacterial adhesion was observed between SWCNTs and MWCNTs. The results of the precipitation assay may be influenced by the aggregation activity of each carbon material, which in turn depends on the differences in their diameters. Bacteria are known to attach to AC particles by means of strong van der Waals forces between the bacterial and the carbon surfaces [11]. Therefore, all types of carbon material will have a high affinity to bacteria because of the generation of van der Waals forces. However, carbon materials with strong aggregation activity, such as SWCNTs, are not readily dispersed in hydrophilic solution and thus, decrease the area available for bacterial adhesion. In contrast, carbon materials with weak aggregation activity, such as 200-MWCNTs and AC, in the limited size range used in this study are not readily precipitated from hydrophilic solution. Our results show 30-MWCNTs had the highest precipitation efficiency, which was attributable to both their adequate dispersibility and aggregation activity.

Subsequently, bacterial adhesion to the CNTs of different diameters in the precipitates was observed by SEM. Fig. 4 shows SEM image of *S. mutans* adhered to CNTs or AC in the precipitates. Several *S. mutans* cells adhered to the meshwork comprising rope-like bundles of SWCNTs, with an average diameter of about 100 nm. Similar to the fibrous shape of the bundles of SWCNTs, fibrous extracellular polymeric substances (width of about 10 nm) were also observed at right-angles to the bacterial surface (the black arrows in Fig. 4). Furthermore, it is notable that some of the bundles wound around the curved surfaces of the *S. mutans* cells (Fig. 4a and b). Thus, the flexibility of the bundles seems to be greater than that of the bacterial cell wall. Sano et al. [12] reported that SWCNTs are worm-like polymers in solution and have flexibility. Therefore, SWCNTs can adjust their structure to follow the surface morphology of *S. mutans* (radius of minor axis: 500 nm). Fig. 4a clearly shows that a bundle of SWCNTs captured *S. mutans* passing through a pore of a membrane filter. A flexible net of SWCNTs can be strongly bent without breaking. In a similar manner, 30-MWCNTs (average diameter of 30 nm) captured *S. mutans* and wound around the curved surface of *S. mutans* (Fig. 4c). Poncharal et al. [13] reported that the ripple structure in the tube caused the MWCNTs (diameter of ~30 nm) to bend uniformly, with a radius of curvature of 400 nm. 30-MWCNTs could wind around the bacteria with the ripple structure. In contrast, though the 200-MWCNTs (average diameter of 200 nm) also adhered to the cells, they did not wind around the surface of *S. mutans* (Fig. 4d). Thus, the flexibility of 200-MWCNTs seems to be less than that of the bacterial cell wall. As for the control material (Fig. 4e), bacterial adhesion occurred at the surface of AC (average particle size 20 μm).

Further, rounded bacteria adhered to SWCNTs under these conditions. This observation contradicts the previous result that flattened cells are inactivated on SWCNTs, which was reported by Kang et al. [9,10] and Brady-Estévez et al. [14]. The differences in morphology could depend on the differences between Gram-positive bacteria, which have a thick cell wall (such as *S. mutans*), and Gram-negative bacteria, which have a thin cell wall (such as *E. coli*), or on the purity of SWCNTs. In addition, CNTs winding around bacteria have not been clearly observed in previous studies [7,9]. This could be explained by the difference between Gram-positive and Gram-negative bacteria or by the use of different procedures for mixing bacteria with CNTs.

In our study, data from both the precipitation assay and SEM images prove that CNTs can adhere to *S. mutans*. Although all types of carbon materials show high affinity toward bacteria because of the generation of van der Waals forces, it has been shown that CNTs of different diameters have significantly different effects on the precipitation efficiency, and the ways in which they capture cells are different. We found that 30-MWCNTs had the highest precipitation efficiency, which was attributable to both their adequate dispersibility and aggregation activity. This may be attributed to differences in the flexibility of the nanotubes. The advantages of capturing pathogens by winding CNTs may be to ensure stronger adhesion and to inhibit the release and budding of captured bacteria. We believe that this could be one of the features of CNTs.

Although the optimum conditions for precipitation are still not clear, we have demonstrated that *S. mutans* can be captured by flexible CNTs. For capturing or eliminating bacteria, the use of CNTs that can adhere to bacteria via physical sorption is not linked to antimicrobial resistance. Bare CNTs having high adhesive ability could be useful as biomaterials, e.g., as tools for the elimination of oral pathogens at the nano-level.

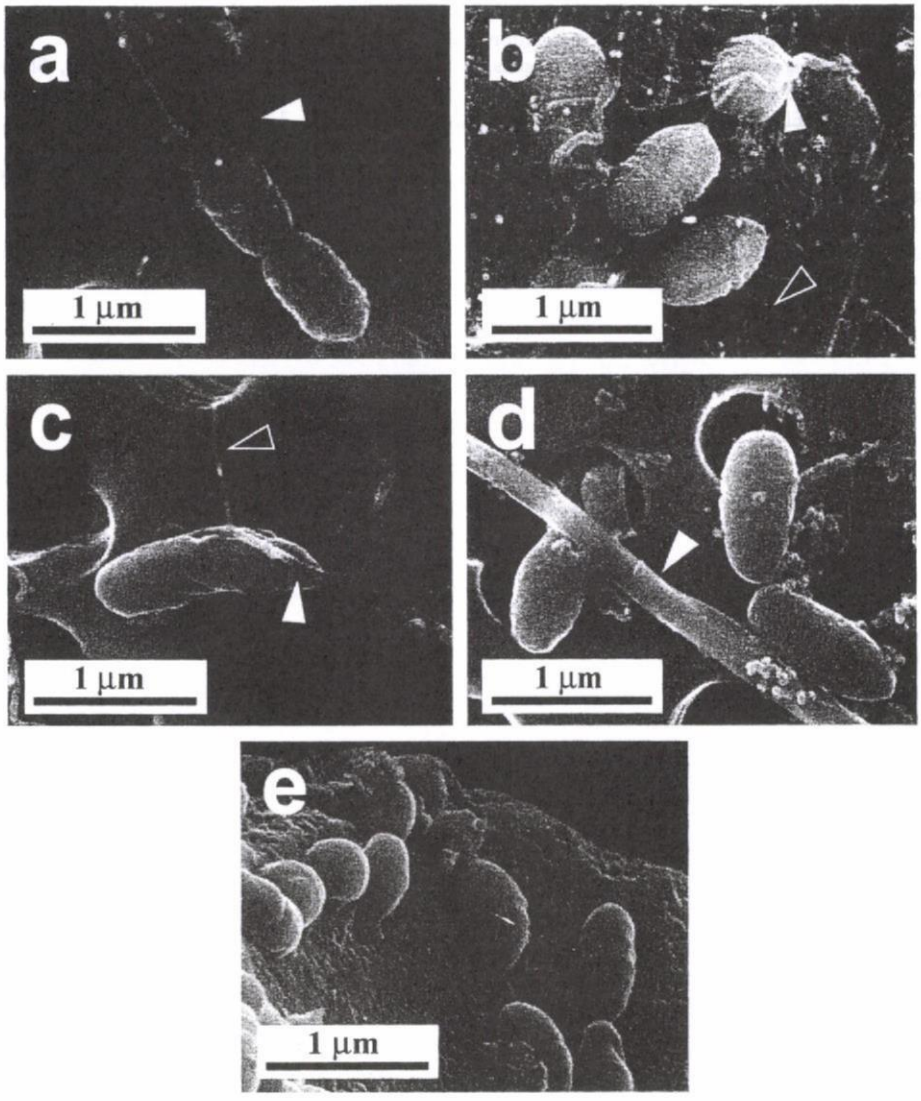

Fig. 4. SEM images of *S. mutans* adhered to CNTs or AC: bundles of SWCNTs wound around *S. mutans* (a); the bacteria adhered to the meshwork comprising bundles of SWCNTs (b); 30-MWCNTs wound around bacteria (c); 200-MWCNTs adhered but did not wind (d); AC surface adhered to bacteria (e). The white arrows indicate CNTs. The black arrows indicate fibrous substances produced by bacteria.

Acknowledgements

We thank Prof. Kazuyuki Tohji and Dr. Yoshinori Sato (Tohoku University) for providing the SWCNTs and Prof. Kenichirou Shibata (Hokkaido University) for donating the *S. mutans* JC2 strain used in this work. This study was supported by Health and Labour Science Research grants in 2006 (H18-kagaku-006) from the Ministry of Health, Labour and Welfare of Japan. Part of this work was also supported by a Grant-in-Aid for Scientific Research (No. 16791177) from the Ministry of Education, Culture, Sports, Science, and Technology of Japan.

References

[1] Pape HL, Solano-Serena F, Contini P, Devillers C, Maftah A, Leprat P. Evaluation of the anti-microbial properties of an activated carbon fibre supporting silver using a dynamic method. Carbon 2002;40:2947–54.

[2] Sarita PT, Tuominen R. Tooth cleaning methods and their effectiveness among adults in rural Tanzania. Proc Finn Dent Soc 1992;88:139–45.

[3] Camper AK, LeChevallier MW, Broadaway SC, McFeters A. Bacteria associated with granular activated carbon particles in drinking water. Appl Environ Microbiol 1986;52:434–8.

[4] Akasaka T, Watari F, Sato Y, Tohji K. Apatite formation on carbon nanotubes. Mater Sci Eng C 2006;26:675–8.

[5] Fugetsu B, Satoh S, Iles A, Tanaka K, Nishi N, Watari F. Encapsulation of multi-walled carbon nanotubes (MWCNTs) in Ba^{2+} -alginate to form coated micro-beads and their application to the pre-concentration/elimination of dibenzo-*p*-dioxin, dibenzofuran, and biphenyl from contaminated water. Analyst 2004;129:565–6.

[6] Srivastava A, Srivastava ON, Talapatra S, Vajtai R, Ajayan PM. Carbon nanotube filters. Nat Mater 2004;3:610–4.

[7] Kim JW, Shashkov EV, Galanzha EI, Kotagiri N, Zharov VP. Photothermal antimicrobial nanotherapy and nanodiagnostics with self-assembling carbon nanotube clusters. Lasers Surg Med 2007;39:622–34.

[8] Zharov VP, Galanzha EI, Shashkov EV, Kim J-W, Khlebtsov NG, Tuchin VV. Photoacoustic flow cytometry: principle and application for real-time detection of circulating single nanoparticles, pathogens, and contrast dyes in vivo. J Biomed Opt 2007;12:051503.

[9] Kang S, Pinault M, Pfefferle LD, Elimelech M. Single-walled carbon nanotubes exhibit strong antimicrobial activity. Langmuir 2007;23:8670–3.

[10] Kang S, Herzberg M, Rodrigues DF, Elimelech M. Antibacterial effects of carbon nanotubes: size does matter! Langmuir 2008;24:6409–13.

[11] Busscher HJ, Dijkstra RJB, Langworthy DE, Collias DI, Bjorkquist DW, Mitchell MD, et al. Interaction forces between waterborne bacteria and activated carbon particles. J Colloid Interface Sci 2008;322:351–7.

[12] Sano M, Kamino A, Okamura J, Shinkai S. Noncovalent self-assembly of carbon nanotubes for construction of "cages". Nano Lett 2002;2:531–3.

[13] Poncharal P, Wang ZL, Ugarte D, de Heer WA. Electrostatic deflections and electromechanical resonances of carbon nanotubes. Science 1999;283:1513–6.

[14] Brady-Estévez AS, Kang S, Elimelech M. A single-walled-carbon-nanotube filter for removal of viral and bacterial pathogens. Small 2008;4:481–4.

Fullerenes, Nanotubes, and Carbon Nanostructures, 16: 114–125, 2008

ISSN 1536-383X print/1536-4046 online
DOI: 10.1080/15363830801887992

Taylor & Francis
Taylor & Francis Group

Carbohydrate Coating of Carbon Nanotubes for Biological Recognition

Tsukasa Akasaka and Fumio Watari

Department of Biomedical Materials and Engineering, Graduate School of Dentistry, Hokkaido University, Sapporo, Japan

Abstract: We have demonstrated that multi-walled carbon nanotubes (MWNTs) coated with a carbohydrate-carrying polymer for use as biological recognition signals can be easily prepared by a non-covalent method via hydrophobic interactions. Fluorescence observation by confocal laser scanning microscopy showed that the carbohydrate-carrying polymers were densely localized around the MWNTs. To evaluate biological recognition affinity, interactions of the MWNTs with lectins were examined by binding tests. The resultant MWNTs were found to acquire a selective binding affinity to the corresponding lectin without a non-specific interaction. On the other hand, bare MWNTs non-specifically interacted with lectins. These results showed that the MWNTs coated with a carbohydrate-carrying polymer have biological recognition signals. Modification of carbon nanotubes with various carbohydrate chains will be a useful protocol for molecular designs of biomaterials, nanoarchitecture and biosensors.

Keywords: Carbon nanotubes, carbohydrate, surface modification, recognition, lectin

INTRODUCTION

Carbon nanotubes (CNTs) have been attracting considerable attention because of their unique physical properties and potential for a variety of applications. Modifications of CNTs by covalent and non-covalent methods have been examined in recent studies (1–6). It is interesting to decorate the open end

Received 9 October 2007, Accepted 2 January 2008
Address correspondence to Tsukasa Akasaka, Department of Biomedical Materials and Engineering, Graduate School of Dentistry, Hokkaido University, 060-8586 Sapporo, Japan. E-mail: akasaka@den.hokudai.ac.jp

or the outer surface of CNTs with biological molecules such as DNA (7, 8), protein (9, 10), enzyme (11, 12), poly- and mono-saccharide (13–18) and others (19, 20). DNA molecules adsorbed on the surface of CNTs via nonspecific interactions have been observed (7). Streptavidin has also been found to adsorb on the surface of CNTs presumably via hydrophobic interactions (9).

Biological functions of carbohydrate chains of glycolipids and glycoproteins have attracted much attention in recent years. Carbohydrate chains are involved in various recognition phenomena, such as fertilization, cell adhesion, tissue formation, antigen-antibody reaction, cancer metastasis and infection of viruses and bacteria (21). More attention has recently been paid to synthetic polymers with pendant carbohydrate chain moieties for use as biological recognition signaling molecules (22). Carbohydrate-carrying polymers have been used as cell-specific culture substrata, in human vaccines, for tumor diagnosis, as probes for receptors, and in targeted drug delivery systems (23–27). These applications are based on biological recognition phenomena, that is, specific interactions between carbohydrates on the polymers and proteins (28–30).

However, no facile method for incorporating carbohydrate chains as recognition signaling molecules into CNTs has been reported. Here we describe a simple method for surface modification of CNTs with carbohydrate chains as recognition signaling molecules. In this study, we used commercially available lactose-carrying polystyrene (PVLA) (31–33), which has both pendant β-galactose moieties for use as recognition signaling molecules and a polystyrene backbone that can be adsorbed onto the surface of CNTs via hydrophobic interactions.

EXPERIMENTAL PROCEDURES

Materials

Poly-(*N*-*p*-vinyl benzyl-*O*-β-D-galactosyl-D-gluconamide) [lactose-carrying polystyrene (PVLA); MW: 5×10^4] and FITC-labeled PVLA were purchased from Seikagaku Corp. (Tokyo, Japan). Rhodamine-labeled *Ricinus communis* agglutinin lectin (Rhod-RCA_{120}, β-galactose-specific lectin) and rhodamine-labeled concanavalin A (Rhod-ConA, α-glucose- or α-mannose-specific lectin) were purchased from VECTOR Laboratories, Inc. (Burlingame, Calif., USA).

Multi-walled carbon nanotubes (MWNTs) used in this study were obtained from two different sources: NanoLab (Brighton, Mass., USA) and MTR Co., Ltd. (Ohio, USA). MWNTs from NanoLab (30-MWNTs; about 30 nm in average diameter) were produced by the chemical vapor deposition (CVD) method, whereas MWNTs from MTR Co. (200-MWNTs; about 200 nm in average diameter) were produced by the arc discharge method. The raw MWNTs were refluxed in 6 N HCl solution and then washed

thoroughly with deionized water and completely dried. 30-MWNTs contain <20% amorphous carbon and 200-MWNTs contain <15% amorphous carbon as the dominant impurity. Typical SEM images of the purified MWNTs are shown in Figure 1.

Preparation of the MWNTs Coated with a Carbohydrate-carrying Polymer

MWNTs material was dispersed in 10 mM phosphate-buffered saline (PBS (+), pH 7.2, 0.5 mL) at a concentration of 50 mg/L by ultrasonication for 15 min. A sufficient amount of PVLA was added to the MWNTs solution to result in a 2% solution by weight, which was then ultrasonicated for 15 min. After 1 h of incubation at room temperature, the mixture was centrifuged (13,000 *g*, 10 min). The aggregated MWNTs were carefully washed three times with PBS and two times with deionized water to remove the unadsorbed polymer.

Interactions with Lectins

A small portion of the MWNTs coated with FITC-PVLA was suspended in 10 mM phosphate-buffered saline (PBS (+), pH 7.2, 0.5 mL). Rhod-RCA_{120} (or Rhod-ConA) was added to a final concentration of 450 nM, and the mixture was then incubated for 1 h at room temperature. After incubation, the mixture was centrifuged (13,000 *g*, 10 min). The aggregated MWNTs were carefully washed three times with PBS and two times with deionized water to remove the uninteracted lectin.

To observe non-specific interactions with lectins, a small portion of bare MWNTs was suspended in PBS. Rhod-RCA_{120} (or Rhod-ConA) was added to a final concentration of 450 nM. After 1 h of incubation at room temperature, the mixture was centrifuged (13,000 g, 10 min). The aggregated MWNTs

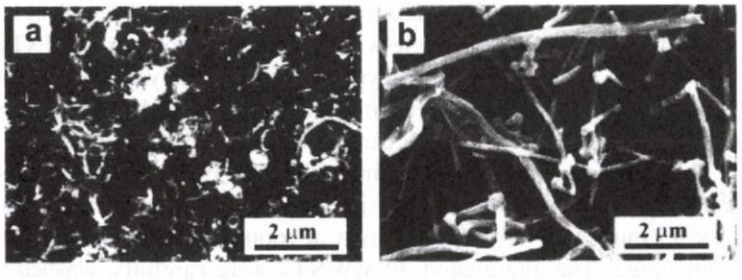

Figure 1. SEM images of the purified MWNTs. a: 30-MWNTs, b: 200-MWNTs.

were carefully washed three times with PBS and two times with deionized water to remove the unadsorbed lectin.

Scanning Electron Microscopy (SEM)

A HITACHI S-4000 scanning electron microscope (HITACHI Instruments, Inc., Tokyo, Japan) was used for SEM.

Fourier Transform Infrared Spectroscopy (FT-IR)

IR absorption spectra were obtained using a JASCO FT/IR-300E fourier transform infrared spectrometer (JASCO, Tokyo, Japan) in the transmission mode on pressed MWNTs pellets mixed with KBr.

Confocal Laser Scanning Microscopy (CLSM)

For CLSM, a small drop of sample solution was placed onto a glass slide, and the solution was covered with a cover glass to prevent evaporation of the solution. CLSM was performed using a Carl Zeiss LSM 410 Axiovert microscope (Carl Zeiss, Oberkochen, Germany) in the transmitted light mode and the fluorescence mode with a 20 × objective at zoom factor 4.8. FITC was excited with a 488-nm argon beam, and emission was collected between 515 and 565 nm. Rhodamine was excited with a 543-nm He-Ne beam, and emission was collected beyond 590 nm. Two different images were acquired from each laser line with green and red colors from FITC and rhodamine, respectively.

RESULTS AND DISCUSSION

Preparation of MWNTs Coated with Carbohydrate-carrying Polymer

In the method reported by O'Connell et al. (34), formation of chemical bonds was substituted by wrapping single-walled carbon nanotubes (SWNTs) in macromolecules such as poly(vinylpyrrolidone) and polystyrene sulfonate molecules. On the basis of their reported method, we used lactose-carrying polystyrene (PVLA) as a model carbohydrate-carrying polymer in this work. The procedure used for coating 30-MWNTs with PVLA was as follows. PVLA and 30-MWNTs material were put into water and ultrasonicated for 15 min. After 1 h of incubation at room temperature, the mixture was centrifuged. The aggregated 30-MWNTs were carefully washed with PBS and deionized water to remove the unadsorbed polymer.